Measurement of cytokine biomarkers using an aptamer-based affinity graphene nanosensor on a flexible substrate toward wearable applications

Journal:	*Nanoscale*
Manuscript ID	NR-ART-05-2018-004315.R1
Article Type:	Paper
Date Submitted by the Author:	01-Oct-2018
Complete List of Authors:	Hao, Zhuang; Harbin Institute of Technology, School of Mechatronics Engineering Wang, Ziran; Columbia University Li, Yijun; Columbia University Zhu, Yibo; Columbia University, Wang, Xuejun; Columbia University De Moraes, Carlos Gustavo; Columbie University Pan, Yunlu; Key laboratory of Micro-Systems and Micro-Structures Manufacturing, Ministry of Education, Harbin Institute of Technology, Harbin 150001, P.R. China,, School of Mechatronics Engineering, Harbin Institute of Technology Zhao, Xuezeng; Key laboratory of Micro-Systems and Micro-Structures Manufacturing, Ministry of Education, Harbin Institute of Technology, Harbin 150001, P.R. China, School of Mechatronics Engineering, Harbin Institute of Technology Lin, Qiao; Columbia University, Dept of Mechanical Engineering

Journal Name

ARTICLE

Measurement of cytokine biomarkers using an aptamer-based affinity graphene nanosensor on a flexible substrate toward wearable applications

Received 00th January 20xx,
Accepted 00th January 20xx

DOI: 10.1039/x0xx00000x

www.rsc.org/

Zhuang Hao,[a,b] Ziran Wang,[a,b] Yijun Li,[a] Yibo Zhu,[a] Xuejun Wang,[a] Carlos Gustavo De Moraes,[c] Yunlu Pan,[b] Xuezeng Zhao[b] and Qiao Lin[a,*]

We present an approach to label-free detection of cytokine biomarkers using an aptamer-functionalized, graphene-based field effect transistor (GFET) nanosensor on a flexible, SiO_2-coated substrate of the polymer polyethylene naphthalate (PEN). The nanosensor conforms to the underlying nonplanar surface and performs GFET-based rapid transduction of the aptamer-biomarker binding, thereby potentially allowing detection of cytokine biomarkers that are sampled reliably from human bodily fluids (e.g., sweat) in wearable sensing applications. In characterizing the suitability of the nanosensor for wearable applications, we investigate the effects of the substrate bending on the equilibrium dissociation constant between the aptamer and the biomarker as well as the graphene transconductance. The utility of the nanosensor is demonstrated by the detection of tumor necrosis factor-α (TNF-α), an inflammatory cytokine biomarker. Experimental results show that the flexible nanosensor can specifically respond to changes in the TNF-α concentration within 5 minutes with a limit of detection as low as 26 pM in a repeatable manner.

1 Introduction

Various health conditions involve abnormal variations in cytokine (6-70 kDa) biomarker concentrations in bodily fluids of patients,[1,2] such as blood,[3] saliva,[4] and sweat.[5] Hence, continuous detection of cytokine biomarker concentrations to inform of inflammatory conditions of patients is highly desirable for early clinical diagnostics. Wearable sensors, which could be attached to the surface of the human body, are considered to be a convenient, effective and viable solution to this need.

Conventionally, cytokine detection is based on methods such as enzyme-linked immunosorbent assay (ELISA) and bead-based immunoassay processes. These methods are well established and effective, but typically require complex sample labelling processes and long assay times (3-8 h).[6] Efforts to address these issues have primarily used optical and electrochemical methods. Optical sensors, relying on detection of cytokine adsorption or cytokine-receptor binding via the induced changes in absorbance,[7] fluorescence,[8] and surface plasmon resonance,[9] can rapidly quantify cytokines in a few minutes.[10] Electrochemical sensors measure the electric current generated from the oxidation or reduction of an electroactive analyte in a chemical reaction, and may provide short response times and higher sensitivities.[8] Unfortunately, these devices mostly require off-line operation,[11] and are based on rigid substrates that do not have mechanical flexibility. Therefore, they are not amenable to further development towards wearable sensing applications, in which continuous inline monitoring of biomarkers on nonplanar surfaces is essential for providing timely information on disease conditions.

Graphene is a two-dimensional nanomaterial that is attractive for detection of biomolecules. In particular, graphene-based affinity sensors, such as aptameric graphene field-effect transistors (GFETs), can enable sensitive and label-free detection of biomarkers in a rapid and continuous manner.[12–15] Moreover, due to the high degree of mechanical flexibility of graphene, GFETs also hold potential in wearable applications. When fabricated on flexible polymer substrates such as polydimethylsiloxine (PDMS)[16] and polyethylene terephthalate (PET),[5,17,18] GFET devices have allowed the detection of ions,[5,18] glucose,[17] bacteria,[19] and proteins.[20] In these devices, however, graphene was in direct contact with the polymer substrates. Organic contaminants that are often present in the substrates can potentially induce unwanted doping in the graphene and decrease its carrier mobility, thereby causing a loss of the sensor sensitivity.

This paper presents an approach to label-free detection of cytokine biomarkers in a specific and continuous manner toward wearable applications. The approach uses a solution-gated GFET nanosensor on a flexible, SiO_2-coated substrate of the polymer

[a] Department of Mechanical Engineering, Columbia University, New York, NY 10027, USA.
Email: qlin@columbia.edu
[b] School of Mechatronics Engineering, Harbin Institute of Technology, Harbin, Heilongjiang 150001, China.
[c] Department of Ophthalmology, Columbia University, New York, NY 10032, USA.
†Electronic Supplementary Information (ESI) available.
See DOI: 10.1039/x0xx00000x

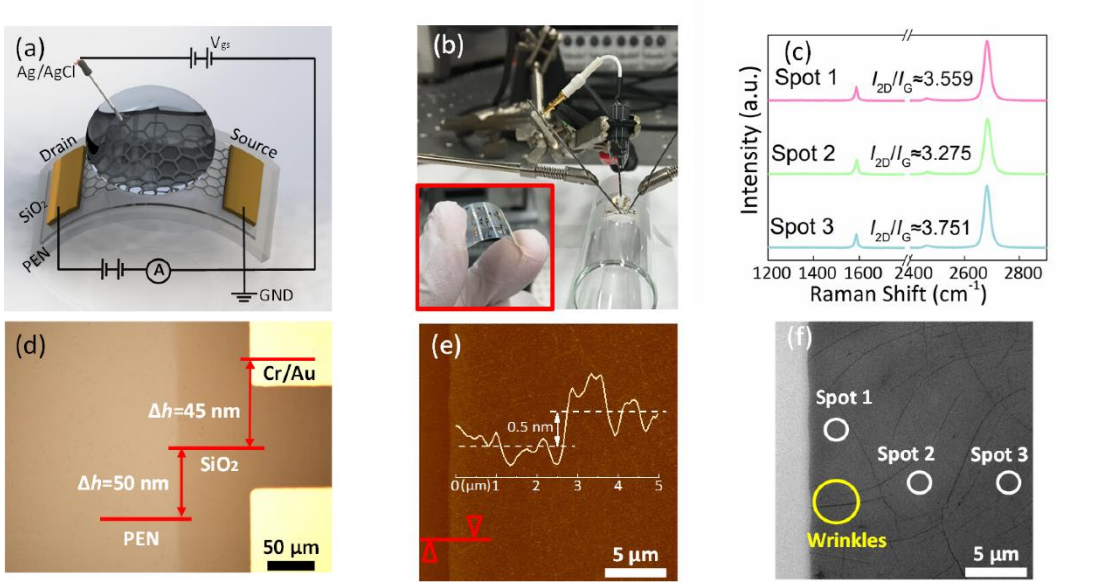

Figure 1 The flexible graphene aptameric nanosensor. (a) Illustration of an electrolyte-gated flexible graphene field-effect transistor. (b) Single flexible nanosensor is equipped with a PDMS microchamber for liquid handling and placed on a nonplanar surface. Inset: Fabricated nanosensors on the PEN film. (c) Raman spectrum of monolayer graphene transferred onto a SiO_2/Si substrate. (d) Micrograph of a SiO_2-coated PEN film integrated with gold electrodes. (e) AFM image of monolayer graphene on a SiO_2/Si substrate. The red line represents a scanning trace of graphene, which is plotted in the inset. (f) SEM image of monolayer graphene on a SiO_2/Si substrate.

polyethylene naphthalate (PEN) (Figure 1). An aptamer is functionalized on the graphene surface and specifically binds with the target biomarker to induce a change in the carrier concentration in the graphene, which is used to determine the cytokine biomarker concentration.

Compared to existing fluorescent and electrochemical cytokine sensors that are based on rigid substrates and are limited to offline operation,[4,21,22] the nanosensor is capable of reliably sampling cytokine biomarkers in human bodily fluids such as sweat by conforming to the underlying nonplanar surface, thereby effectively addressing issues related to rigid sensors such as limited secretion and evaporation of sweat. In addition, the device operates continuously and in real time by GFET-enabled rapid transduction of the affinity recognition of the biomarkers. The implementation of the nanosensor is based on a flexible PEN substrate, which offers excellent chemical stability and biocompatibility,[18,20,23] and the coating of PEN by SiO_2 protects the graphene from potential unwanted doping of contaminants within PEN. The affinity recognition of the biomarkers is achieved using a short DNA aptamer (e.g., consisting of 25 nucleotides) as a cytokine-specific receptor. Compared with receptors (e.g., antibodies) that have much larger sizes, the short aptamer can bring the charged cytokine molecule more closely to the graphene surface upon affinity binding, thereby enhancing the sensitivity of cytokine detection. Further, compared with antibody-based flexible cytokine sensors, of which the antibody-antigen interaction is weakened with increasing storage time,[24,25] the aptamer employed in our nanosensor offers higher stability and consistency even after extended-time storage. The nanosensor is characterized in relation to its suitability for wearable applications, such as the effects of the substrate bending on the equilibrium dissociation constant between the aptamer and the biomarker as well as the graphene transconductance, which is the primary indicator of the sensitivity of the nanosensor. These characteristics, which have not been investigated for existing flexible GFET sensors,[18,23] are critical for ensuring that the nanosensor can operate reliably and consistently in the presence of frequent, significant bending caused by the movement of the patient body.

We demonstrate the approach using TNF-α, an inflammatory cytokine biomarker closely related to conditions such as fever, Crohn's disease, and pulmonary tuberculosis, as a representative cytokine biomarker. Experimental results show that our flexible nanosensor can specifically respond to changes in the TNF-α concentration within 5 minutes，which was 6 times shorter than existing TNF-α detection methods using aptamers,[4,21] with a limit of detection down to 26 pM in a repeatable manner. These results demonstrate that the nanosensor offers the flexibility and consistency required to enable detection of cytokine biomarkers in sweat in wearable sensing format.

Results and discussion

To examine the effectiveness of the SiO_2 isolation nanolayer, which was coated on the PEN substrate not only to protect graphene from the potential doping effect induced by organic contaminations in PEN but also to provide a smoother surface for the nanosensor fabrication, graphene electrical properties were investigated after transferring graphene onto bare PEN and 50 nm thick SiO_2 coated PEN separately. Graphene transfer curves were measured using multiple devices with or without coated SiO_2 nanolayer and plotted in Figure 2a. It is observed that the transconductance of hole and

electron conduction branches in the transfer curve are enhanced by 52.26% and 216.78%, respectively (Figure 2b). Meanwhile, the average value of the surface roughness is also found to be improved from 10.82 nm to 3.64 nm (Figure 2c, d).

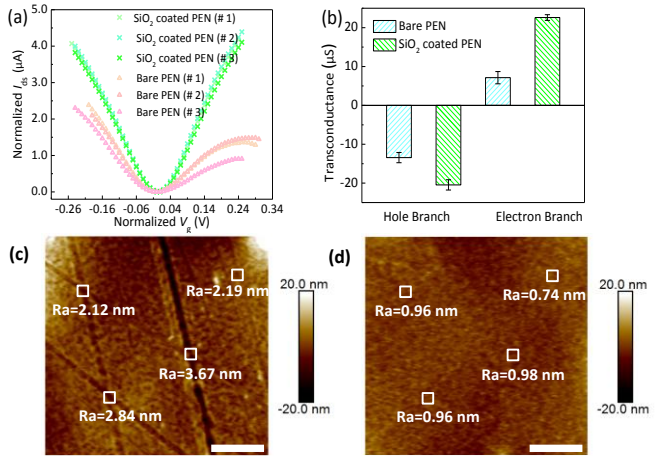

Figure 2 Surface and electrical characterization of the nanosensor. (a) Transfer characteristic curves of graphene on bare PEN and PEN coated with 50 nm-thick SiO_2 (measured at V_{ds}=0.01V). (b) Comparison of the graphene transconductance on different substrates. (c, d) Surface morphology of bare PEN and 50 nm thick SiO_2 layer coated PEN obtained by AFM (Scale bar: 1 μm).

Therefore, the SiO_2 isolation nanolayer is likely to provide a more appropriate surface for placing the graphene-based nanosensor.

To assess the mechanical flexibility and the sensing consistency of the nanosensor, electrical behaviors of the nanosensor was tested with different outward and inward directional bending curvatures. First, we measured the graphene conductivity by fixing the flexible nanosensor onto nonplanar rigid surfaces with different inward and outward bending radii (flat, 40.3, 24.6, 17.3 and 8.1 mm) (Figure S4). It is observed that the graphene resistance and the Dirac point V_{Dirac}, where I_{ds} reaches its minimum in the transfer curve, has significant and unidirectional changes by 17.30% (16.55%) and -0.073 V (-0.042 V) with respect to the decreasing outward (inward) bending radii from flat to 8.1 mm, respectively (Figure S4 a, b, c, d). With increasing applied tensile and compressive strain, the crystal structure of graphene is distorted, breaking the crystal symmetry and modifying the electronic band structure of graphene, which will also split the degeneracy of energy bands and weak the electron transmission near Fermi level and result in the observed increase of resistance and negative shift of the Dirac points.[26,27] The previous work, in which the resistance of graphene increases from 492 to 522 kΩ with applied strain up to 1%, also supports our experimental results.[28] Instead, the transconductance in two conduction branches of the transfer curve are almost invariable, the ratio of the transconductance measured at different outward (inward) bending status, $g_{m\text{-}i}$, and the transconductance measured under flat status, $g_{m\text{-}flat}$, is almost kept constant at 1.0 (fluctuation less than 0.1) with applied strain up to 0.8% at a bending radius of 8.1 mm (Figure S4 e, f). This can be explained as that in spite of the additional scattering and reduction in the carrier mobility resulted from the crystal distortion of graphene in the reversible deformation range, the crystal structure of graphene still maintains its hexagonal honeycomb crystal structure.[29] Therefore, the weak variation in the carrier mobility of graphene is not likely to cause significant change in the transconductance of graphene at an applied strain under 5%. In addition, the same measurement was carried out again after relaxing the flexible nanosensor back to flat for 15 min. As a consequence, no obvious variation in the graphene conductivity is observed after relaxing processes from outward (inward) bending status. The original resistance and the Dirac point could almost both be restored even for a bending radius down to 8.1 mm, whereas the transconductance, a critical sign of the nanosensor sensitivity, is almost constant all the time (Figure 3). These experimental results are in good agreement with related studies[28] that the lattice distortion of graphene could be entirely recovered after removing applied strain less than 5% and indicate that the flexible nanosensor offers not only good mechanical flexibility but also well stability, thus opening up the possibility for reliable biosensing in both flat and bent status.[18,20]

The inertness of graphene to TNF-α was manifested by exposing the graphene channel to TNF-α solutions without prior biofunctionalization of graphene. The V_{Dirac} is not seen to have distinguishable shift with exposure to TNF-α solutions with increasing concentrations (0 to 1 μM) (Figure S5). Due to the low molecular mass of TNF-α (17.48 kDa), TNF-α is more likely not to adsorb onto untreated graphene at clinically relevant concentrations in the detection time (<10 min) or the adsorption does not alter the graphene conductivity significantly.[14] Hence, graphene is appropriate for the TNF-α detection.

Characterization of electrical properties of the nanosensor was performed to verify the successful biochemical functionalization

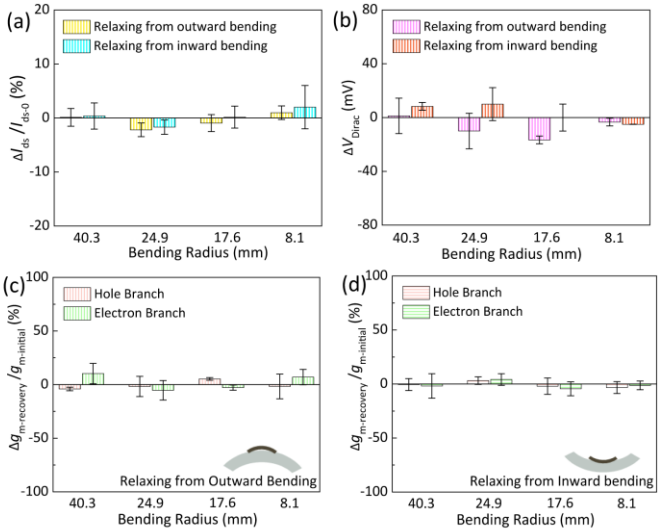

Figure 3 Comparison of graphene electrical properties before and after PEN substrate bending. Changes (compared with the original data before PEN bending) are shown the resistance (a), the Dirac point (b) and the transconductance (c, d) of graphene after recovery (for 15 min) from outward and inward bending at different radii of curvature (measured at V_{ds}=0.01V).

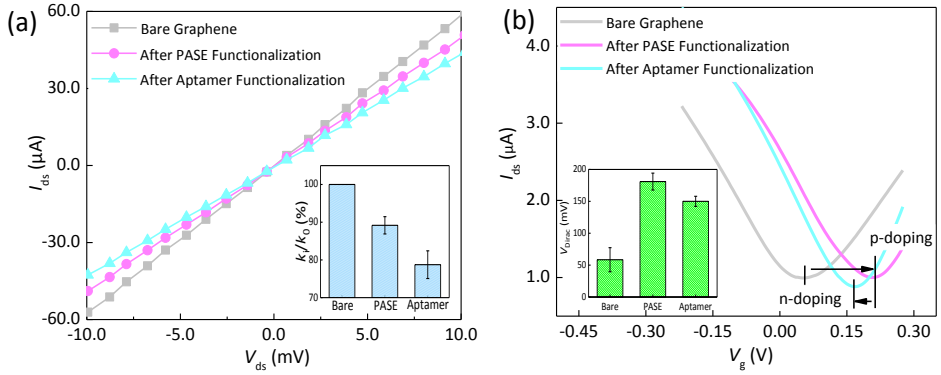

Figure 4 Characterization of the biochemical functionalization of the nanosensor. (a) Current-voltage curves before and after PASE and aptamer functionalization. Inset: Slope of current-voltage curves before and after PASE and aptamer functionalization. (b) Transfer characteristics of graphene before and after each functionalization step. Inset: The position of Dirac point before and after PASE and aptamer functionalization.

after each immobilization step of PASE and aptamer VR11. First, the output characteristics of the flexible nanosensor were measured at different V_g from -0.3 V to 0.2 V in a step of 0.1 V and shown in Figure S6. It is found that the dI_{ds}/dV_{ds} value decreases by 54.47% with positive increasing V_g. However, the I_{ds}-V_{ds} relation remains linear, suggesting that highly stable ohmic contact between graphene and golden electrodes is preserved.[18,20] Hence, electrostatic gating effect of the graphene channel, rather than the contact resistance, is likely to be the dominant effect resulting in the electrical current changes in the GFET flexible nanosensor. Subsequently, the I_{ds}, corresponding to different graphene functionalization steps, was measured with V_{ds} increasing from -10 mV to 10 mV by fixing V_g at 0 V. It is seen that the dI_{ds}/dV_{ds} value decreases by 10.83% and 21.26% after PASE and aptamer VR11 immobilization, respectively (Figure 4a). Additionally, the coupling of PASE to the graphene surface is observed to increase V_{Dirac} from 58 to 181 mV, indicating that PASE induced p-type doping to graphene.[30] However, V_{Dirac} is decreased down to 150 mV after the treatment of aptamer VR11 (Figure 4b). Considering these results, it can be concluded that the functionalization of aptamer VR11 is successful.

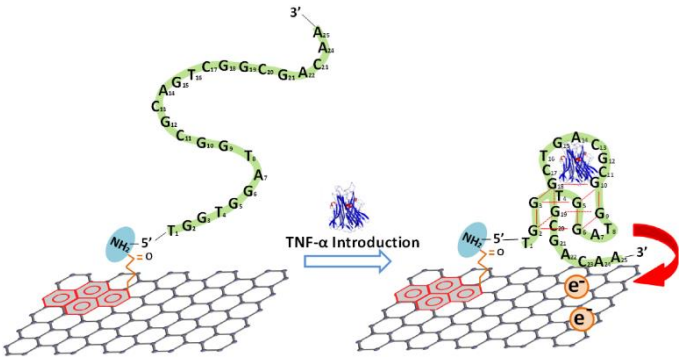

Schematic 1 Principle of the GFET nanosensor for TNF-α detection. The aptamer specifically binds to TNF-α, switching to a stable and compact G-quadruplex formation, bringing negatively charged TNF-α and oligonucleotide strands to the close vicinity of the graphene surface, thereby altering the carrier concentration in the graphene and yielding detectable signals.

Detection of TNF-α is allowed by the structural change of its graphene surface immobilized specific aptamer VR11 when interacting with TNF-α (Schematic 1). Aptamer VR11 is a single strand oligonucleotide, which folds into a compact and stable guanine quadruplexes (G-quadruplex) formation composed of two guanine tetrads from loop, flexible state upon affinity binding with TNF-α. These structural changes of the aptamer in the close proximity of the graphene surface cause disturbances to the charge carrier concentration in graphene and result in detectable changes in the measured I_{ds}.

To elucidate the TNF-α measuring capabilities of the flexible nanosensor, TNF-α solutions (diluted in 1X PBS buffer) of increasing concentrations from 50 pM to 500 nM were sequentially introduced to the PDMS chamber that attached on top of the graphene channel for liquid handling. The affinity binding process of TNF-α to aptamer VR11 was allowed to reach equilibrium before the replenishment of a higher concentration specimen solution. All measured graphene ambipolar transfer curves were obtained by increasing V_g from 0 to 0.4 V with a constant V_{ds}=10 mV. After exposure to TNF-α solutions, the transfer curve is observed to shift negatively and dramatically (Figure 5a). The carrier mobility of graphene is not likely to be altered significantly by the TNF-α–aptamer binding, which is in agreement with our experimental result that the transconductance of both hole and electron conduction branches remains constant, at ~37.6 μS and ~46.5 μS, respectively. In contrast, V_{Dirac} is decreased by 25.5 mV and down to a value of 40.5 mV within physiologically relevant TNF-α levels (0 to 200 pM), suggesting that more electrons (n-type carriers) are doped into graphene upon the interaction of TNF-α to aptamer VR11, thus generating n-type doping to graphene. Given that the isoelectric point (PI) of TNF-α is between 4.0~5.0, the TNF-α molecule is deemed negatively charged in 1X PBS buffer at pH 7.4. In the absence of the TNF-α target molecule, the guanine rich aptamer VR11 is mostly unfolded and flexible in the solution. Upon binding with TNF-α, the oligonucleotide strands immediately fold to stable and compact G-quadruplex formations,[15] bringing the electron-rich

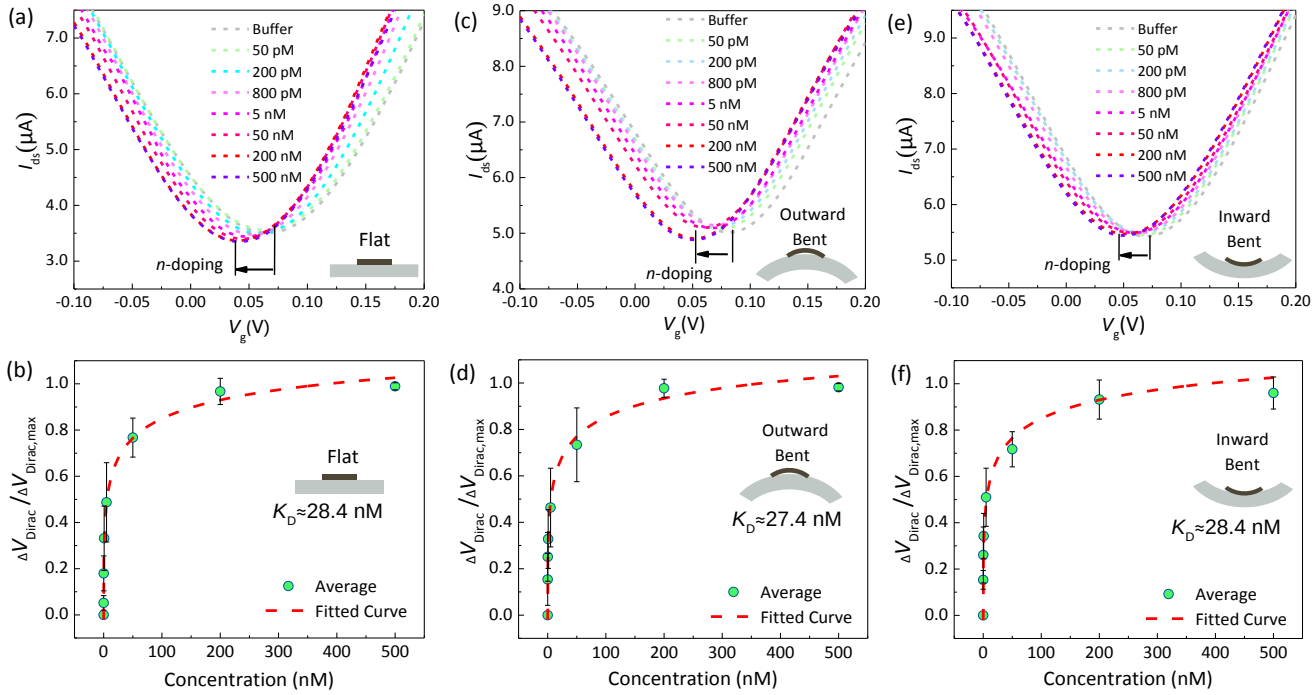

Figure 5 Detection of TNF-α using the flexible aptameric nanosensor. (a, c, e) Transfer characteristics measured when the aptamer- functionalized graphene were exposed to TNF-α solutions (concentration: 50 pM to 500 nM) with the substrate bent at different radii of curvature. (b, d, f) Voltage shift ΔV_{Dirac} as a function of the TNF-α concentration. The dashed line is a least-squares fit to the Hill-Langmuir equation, yielding an equilibrium dissociation constant (K_D) of 28.4, 27.4 and 28.4 nM for flat, outward bending and inward bending of the substrate, respectively.

aromatic oligonucleotide strands with strongly and negatively charged TNF-α molecules to the close vicinity of graphene and possibly making the nucleotide or aromatic amino acids on TNF-α directly bind to graphene. As a result, electrons from not only TNF-α but also the deformed aptamer VR11 are more likely to be directly transferred into graphene through the π–π stacking interactions, thus generating n-type doping to graphene and altering the carrier concentration in graphene. This mechanism was also reported in previous works[13,31] and considered to serve as the underlying biosensing principle that allows us to detect TNF-α.

In addition, the affinity binding dissociation constant (K_D) for aptamer VR11 and TNF-α was estimated with the V_{Dirac} values obtained at corresponding TNF-α concentrations. Here, the variation in V_{Dirac}, denoted as ΔV_{Dirac}, is plotted as a function of TNF-α concentrations and shown in Figure 5b (Error bars represented the maximum and minimum values were obtained from multiple measurements). The ΔV_{Dirac} is found to increase sharply with increasing TNF-α concentrations from 50 pM to 200 nM and then becomes unchanged and stable afterwards. A Hill–Langmuir relationship can be used to accurately describe the affinity binding of aptamer VR11 with TNF-α. To address device-to-device non-uniformities resulting from variations in fabrication processes and material properties, the device output is normalized using the formula $\Delta V_{Dirac}/\Delta V_{Dirac,max}$ with $\Delta V_{Dirac,max} = V_{Dirac,max} - V_{Dirac,0}$, where $V_{Dirac,0}$ and $V_{Dirac,max}$ are the Dirac point voltage values obtained at a TNF-α concentration of 0 and 500 nM (the maximum concentration tested), respectively. Based on the fitted curves shown in Figure 5b,

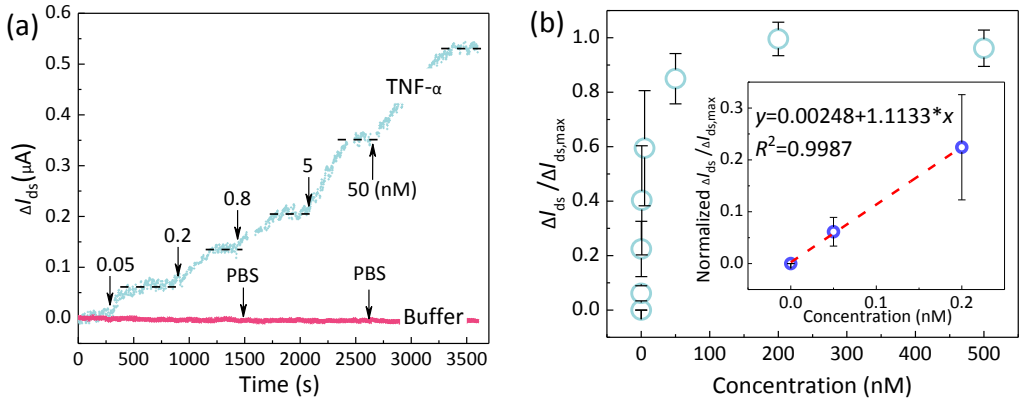

Figure 6 Time-resolved measurement of TNF-α concentrations. (a) Real-time monitoring of changes in the TNF- α concentration. The responses are represented by the changes of the drain–source current I_{ds}. (b) Decrease of the drain–source current with increasing TNF- α concentration. Inset: Linear fit of the drain–source current with increasing TNF- α concentration from 0 to 200 pM.

K_D is estimated to be 28.4 nM, demonstrating a high affinity between aptamer VR11 and TNF-α (Details can be found in Supporting Information). Further, to evaluate the feasibility of the nanosensor using as a flexible TNF-α sensing platform, the same measurement done under the flat condition was repeated by deforming and fixing the flexible nanosensor onto nonplanar rigid surfaces (the bending radius was 40.3 mm).[17] The sensing performance for the flexible nanosensor in outward bent status was assessed (Figure 5c). The profile of changes in the conductivity is similar to those measured under the flat nanosensor condition. The V_{Dirac} is shifted to negative by 29.5 mV with TNF-α concentration increasing from fresh to 500 nM. Instead, the change in the transconductance of both hole and electron conduction branches are still to be negligible and kept less than 5.09% and 4.39%, respectively. In this outward bending situation, K_D is calculated to be 27.4 nM with the fitted curve (Figure 5d). Moreover, all detection experiments were carried out again with an inward bending nanosensor at a fixed bending radius of 40.3 mm. Similar physical phenomena are observed and K_D is estimated to be 28.4 nM (Figure 5e, f). Considering these experimental results, the difference of the sensing performance for the flexible nanosensor using in various bending conditions is relatively small. T Therefore, we can conclude that the flexible nanosensor holds a high level of mechanical flexibility as well as reliability and consistency for the detection of TNF-α.

Continuous time-resolved response to the presence of TNF-α was characterized with fixed V_{ds}=10 mV and V_g=0 V. Starting with 1X PBS solution, 50 pM TNF-α solution as first injected at 300 s and replenished with a higher concentration sample after each binding equilibrium at corresponding concentration thereafter. The measured I_{ds} presents a unidirectional decrease by 0.62 μA. The binding process can reach equilibrium within 350s at corresponding clinically relevant TNF-α levels, enabling the nanosensor for near real-time monitoring TNF-α (Figure 6a). Additionally, a near linear relationship between the change in I_{ds}, denoted as ΔI_{ds}, and TNF-α concentrations can be observed (Figure 6b). Given a noise level of 9.57 nA, the limit of detection (LOD) is estimated to be 25.8 pM. Thus, our GFET nanosensor overall offers a lower detection limit and shorter assay time for detecting TNF-α than most of the existing methods (Table 1).

Table 1. Comparison of the Response Characteristics of the Nanosensor and Other Detection Methods

Receptor	Methods	Assay Time	Limit of detection	Ref.
Nano TNF-α	Reflectometric interference specoscopy	25 min	56 ng/mL	32
Antibody	Quartzy crystal microbalance	10~15 min	25 ng/mL	33
Antibody	Potentiometric sensor	4 min	15 ng/mL	34
Aptamer	Electrochemical sensor	15 min	10 ng/mL	35
Aptamer	Electrochemical sensor	30 min	5.46 ng/mL	21
Aptamer	Microfluidic sensor	30 min	5 ng/mL	36
Antibody	Photonic microring resonator	5 min	4.6 ng/mL	37
Aptamer	Photoluminescence spectroscopy	N/A	1.7 ng/mL	38
Aptamer	Graphene field effect transistor (GFET）	5 min	0.45 ng/mL (26 pM)	This work

The selectivity of the nanosensor was examined using closely related analogues IL-002 and IFN-γ, sharing similar physical structures with TNF-α, as the negative control molecules. 1X PBS, 0.05, 5, 500 and 1000 nM IL-002 or IFN-γ solutions were sequentially introduced to the biochemical functionalized graphene channel. The gaphene transfer curve was measured after corresponding solution replenishment. As shown in Figure 7b, the normalized device output, $\Delta V_{Dirac}/V_{Dirac, PBS}$, where $V_{Dirac, PBS}$ is the Dirac point voltage measured in PBS buffer, is plotted as a function of the concentration of the analyte (TNF-α, IL-002 or IFN-γ). (Error bars are obtained from measurements using three different devices.) It is observed that $\Delta V_{Dirac}/V_{Dirac, PBS}$ fluctuates around 0 with IL-002 or IFN-γ at different concentrations. In contrast, $\Delta V_{Dirac}/V_{Dirac, PBS}$ increases monotonically and sharply with TNF-α concentrations. For TNF-α, the $\Delta V_{Dirac}/V_{Dirac, PBS}$ value at 500 nM (28.2%) is over 5 times greater than that for IFN-γ (5.1%) or IL-002 (0.8%) at the same concentration. The result indicates that a high specificity to TNF-α is achieved by the nanosensor using aptamer VR11.[16]

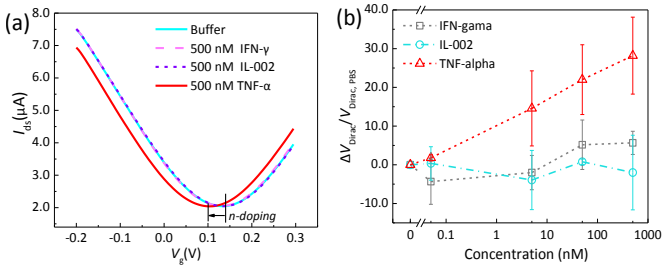

Figure 7 Selective response of the flexible nanosensor to TNF- α. Transfer curves of graphene (a) and normalized changes in the Dirac point (b) with the graphene channel exposed to given solutions (IL-002, IFN- γ or TNF-α).

Conclusions

We have presented an approach for label-free and continuous detection of cytokine biomarkers toward wearable applications and demonstrated its utility with TNF-α. The approach uses a GFET nanosensor on a flexible, 50 nm SiO_2-coated substrate of the PEN. The coating of PEN by SiO_2 protects the graphene from potential unwanted doping of contaminants within PEN. The aptamer VR11 immobilized on the graphene surface specifically binds with TNF-α to induce a change in the carrier concentration in the graphene, which is used to determine the TNF-α concentration. The

nanosensor is capable of reliably sampling TNF-α in human bodily fluids such as sweat by conforming to the underlying nonplanar surface due to the its mechanical flexibility and operates continuously and in real time by GFET-enabled rapid transduction of the affinity recognition of TNF-α. Furthermore, the short (25-base) aptamer VR11 can bring the charged TNF-α more closely to the graphene surface upon affinity binding, thereby enhancing the sensitivity of GFET for TNF-α detection. The effects of the substrate bending on the equilibrium dissociation constant between the aptamer VR11 and TNF-α as well as the graphene transconductance, which are indicators of the suitability of the nanosensor for wearable applications, are characterized. These characteristics are critical for ensuring that the nanosensor can operate reliably and consistently in the presence of frequent, significant bending caused by the movement of the underlying human body. Experimental results show that our flexible nanosensor can specifically respond to changes in the TNF-α concentration within 5 minutes, which is 6 times shorter than previously reported aptameric electrochemical devices, with a limit of detection down to 26 pM in a repeatable manner. This demonstrates the potential utility of the nanosensor for continuous monitoring of cytokines in wearable applications.

Methods

Materials: Chemical vapor deposition graphene was purchased from Graphenea (Cambridge, MA). PEN films (125 μm thick) were ordered from Dupont Teijin Films (Chester, VA). Polydimethylsiloxane (PDMS, SYLGARD-184) was purchased from Dow Corning (Midland, MI) for the PDMS chamber. 1-Pyrenebutanoic acid succinimidyl ester (PASE), phosphate buffered saline (PBS), human Interleukin-002 (IL-002) and human Interferon-γ (IFN-γ) were purchased from Sigma-Aldrich (St. Louis, MO). Human TNF-α was purchased from R&D Systems (Minneapolis, MN). TNF-α-specific aptamer (VR11, sequence 5'-NH_2- TGG TGG ATG GCG CAG TCG GCG ACA A -3')[39] was synthesized and purified by Integrated DNA Technologies (Coralville, IA).

Fabrication: The flexible PEN film was first coated with a 50 nm thick SiO_2 isolation nanolayer by sputtering. Drain and source electrodes (2 nm Cr/43 nm Au) were subsequently fabricated using E-beam evaporation and standard photolithography techniques. The distance between the drain and source electrodes was chosen to be 40 μm. Graphene was then transferred onto the 50 nm SiO_2-coated PEN substrate.

Graphene was next biochemically functionalized. PASE was noncovalently coupled to the graphene surface via π–π interaction, after which the VR11 aptamer was attached to the graphene via the reaction of an amine group on the VR11 aptamer with the N-hydroxysuccinimide ester on PASE. Further details for the device fabrication and graphene surface functionalization can be found in Supporting Information.

Measurements: The GFET-based electrical measurements were performed with the aid of a custom-designed LabVIEW program. Two digital sourcemeters (Keithley 2400, Tektronix) supplied both the drain-source and gate voltages and simultaneously measured the drain-source current I_{ds}.

Conflicts of interest

The authors declare no competing financial interest.

Acknowledgements

This work was supported by funding from the National Institutes of Health (Grant Nos. 1DP3DK101085-01 and 1R33CA196470-01A1) and the National Science Foundation (Grant No. ECCS-1509760). The authors would like to thank Dr. Leejee H. Suh at the Columbia University Medical Center for insightful discussions. Z. Hao and Z. Wang also gratefully acknowledge a National Scholarship (award numbers 201506120133 and 201706120141) from the China Scholarship Council.

References

1 J. A. Gasche, J. Hoffmann, C. R. Boland and A. Goel, *Int. J. Cancer*, 2011, **129**, 1053–1063.
2 D. L. Mann, *Circ. Res.*, 2002, **91**, 988–998.
3 E. Stern, A. Vacic, N. K. Rajan, J. M. Criscione, J. Park, B. R. Ilic, D. J. Mooney, M. A. Reed and T. M. Fahmy, *Nat. Nanotechnol.*, 2010, **5**, 138–142.
4 F. G. Bellagambi, A. Baraket, A. Longo, M. Vatteroni, N. Zine, J. Bausells, R. Fuoco, F. Di Francesco, P. Salvo, G. S. Karanasiou, D. I. Fotiadis, A. Menciassi and A. Errachid, *Sensors Actuators, B Chem.*, 2017, **251**, 1026–1033.
5 W. Gao, S. Emaminejad, H. Y. Y. Nyein, S. Challa, K. Chen, A. Peck, H. M. Fahad, H. Ota, H. Shiraki, D. Kiriya, D. H. Lien, G. A. Brooks, R. W. Davis and A. Javey, *Nature*, 2016, **529**, 509–514.
6 Y. Park, B. Ryu, B. R. Oh, Y. Song, X. Liang and K. Kurabayashi, *ACS Nano*, 2017, **11**, 5697–5705.
7 M. Singh, J. Truong, W. B. Reeves and J. I. Hahm, *Sensors (Switzerland)*, , DOI:10.3390/s17020428.
8 Y. Yang and W. Gao, *Chem. Soc. Rev.*, , DOI:2018/CS/C7CS00730B.
9 J. N. Anker, W. P. Hall, O. Lyandres, N. C. Shah, J. Zhao and R. P. Van Duyne, *Nat. Mater.*, 2008, **7**, 442–453.
10 T. G. Cha, B. A. Baker, M. D. Sauffer, J. Salgado, D. Jaroch, J. L. Rickus, D. M. Porterfield and J. H. Choi, *ACS Nano*, 2011, **5**, 4236–4244.
11 M. Bariya, H. Y. Y. Nyein and A. Javey, *Nat. Electron.*, 2018, **1**, 160–171.
12 C. Wang, Y. Li, Y. Zhu, X. Zhou, Q. Lin and M. He, *Adv. Funct. Mater.*, 2016, **26**, 8575.
13 B. Cai, S. Wang, L. Huang, Y. Ning, Z. Zhang and G. J. Zhang, *ACS Nano*, 2014, **8**, 2632–2638.
14 Z. Hao, Y. Zhu, X. Wang, P. G. Rotti, C. Dimarco, S. R. Tyler, X. Zhao, J. F. Engelhardt, J. Hone and Q. Lin, *ACS Appl. Mater. Interfaces*, 2017, **9**, 27504–27511.
15 Y. Li, C. Wang, Y. Zhu, X. Zhou, Y. Xiang, M. He and S. Zeng, *Biosens. Bioelectron.*, 2017, **89**, 758–763.

16 S. Farid, X. Meshik, M. Choi, S. Mukherjee, Y. Lan, D. Parikh, S. Poduri, U. Baterdene, C. E. Huang, Y. Y. Wang, P. Burke, M. Dutta and M. A. Stroscio, *Biosens. Bioelectron.*, 2015, **71**, 294–299.
17 Y. H. Kwak, D. S. Choi, Y. N. Kim, H. Kim, D. H. Yoon, S. S. Ahn, J. W. Yang, W. S. Yang and S. Seo, *Biosens. Bioelectron.*, 2012, **37**, 82–87.
18 J. H. An, S. J. Park, O. S. Kwon, J. Bae and J. Jang, *ACS Nano*, 2013, **7**, 10563–10571.
19 M. S. Mannoor, H. Tao, J. D. Clayton, A. Sengupta, D. L. Kaplan, R. R. Naik, N. Verma, F. G. Omenetto and M. C. McAlpine, *Nat. Commun.*, 2012, **3**, 763–768.
20 O. S. Kwon, S. J. Park, J. Y. Hong, A. R. Han, J. S. Lee, J. S. Lee, J. H. Oh and J. Jang, *ACS Nano*, 2012, **6**, 1486–1493.
21 Y. Liu, Y. Liu, Z. Matharu, A. Rahimian and A. Revzin, *Biosens. Bioelectron.*, 2015, **64**, 43–50.
22 Y. Liu, T. Kwa and A. Revzin, *Biomaterials*, 2012, **33**, 7347–7355.
23 N. Petrone, T. Chari, I. Meric, L. Wang, K. L. Shepard and J. Hone, 2015, 8953–8959.
24 R. D. Munje, S. Muthukumar, B. Jagannath and S. Prasad, *Sci. Rep.*, , DOI:10.1038/s41598-017-02133-0.
25 K. I. Papamichael, M. P. Kreuzer and G. G. Guilbault, *Sensors Actuators, B Chem.*, 2007, **121**, 178–186.
26 V. M. Pereira, A. H. Castro Neto and N. M. R. Peres, *Phys. Rev. B - Condens. Matter Mater. Phys.*, 2009, **80**, 1–8.
27 Y. Liu, Y. Y. Li, S. Rajput, D. Gilks, L. Lari, P. L. Galindo, M. Weinert, V. K. Lazarov and L. Li, *Nat. Phys.*, 2014, **10**, 294–299.
28 Y. Lee, S. Bae, H. Jang, S. Jang, S.-E. Zhu, S. H. Sim, Y. Il Song, B. H. Hong and J.-H. Ahn, *Nano Lett.*, 2010, **10**, 490–3.
29 D. Choi, M. Y. Choi, W. M. Choi, H. J. Shin, H. K. Park, J. K. Seo, J. Park, S. M. Yoon, S. Chae, Y. H. Lee, S. W. Kim, J. Y. Choi, S. Y. Lee and J. M. Kim, *Adv. Mater.*, 2010, **22**, 2187–2192.
30 Y. Zhu, Y. Hao, E. A. Adogla, J. Yan, D. Li, K. Xu, Q. Wang, J. Hone and Q. Lin, *Nanoscale*, 2016, **8**, 5815–5819.
31 A. Star, E. Tu, J. Niemann, J.-C. P. Gabriel, C. S. Joiner and C. Valcke, *Proc. Natl. Acad. Sci.*, 2006, **103**, 921–926.
32 R. Say, S. E. Diltemiz, S. Çelik and A. Ersöz, *Appl. Surf. Sci.*, 2013, **275**, 233–238.
33 Y. K. Bahk, H. H. Kim, D. S. Park, S. C. Chang and J. S. Go, *Bull. Korean Chem. Soc.*, 2011, **32**, 4215–4220.
34 R. Say, E. B. Özkütük, Ö. B. Ünlüer, D. Uğurağ and A. Ersöz, *Sensors Actuators, B Chem.*, 2015, **209**, 864–869.
35 Y. Liu, Q. Zhou and A. Revzin, *Analyst*, 2013, **138**, 4321–4326.
36 T. Kwa, Q. Zhou, Y. Gao, A. Rahimian, L. Kwon, Y. Liu and A. Revzin, *Lab Chip*, 2014, **14**, 1695–1704.
37 M. S. Luchansky and R. C. Bailey, *J. Am. Chem. Soc.*, 2011, **133**, 20500–20506.
38 S. Ghosh, D. Datta, S. Chaudhry, M. Dutta and M. A. Stroscio, *IEEE Trans. Nanobioscience*, 2018, **PP**, 1.
39 E. W. Orava, N. Jarvik, Y. L. Shek, S. S. Sidhu and J. Gariépy, *ACS Chem. Biol.*, 2013, **8**, 170–178.